Endothelial SHIP2 Suppresses Nox2 NADPH Oxidase–Dependent Vascular Oxidative Stress, Endothelial Dysfunction, and Systemic Insulin Resistance

Nicole T. Watt,[1] Matthew C. Gage,[1] Peysh A. Patel,[1] Hema Viswambharan,[1] Piruthivi Sukumar,[1] Stacey Galloway,[1] Nadira Y. Yuldasheva,[1] Helen Imrie,[1] Andrew M.N. Walker,[1] Kathryn J. Griffin,[1] Natalia Makava,[1] Anna Skromna,[1] Katherine Bridge,[1] David J. Beech,[1] Stéphane Schurmans,[2] Stephen B. Wheatcroft,[1] Mark T. Kearney,[1] and Richard M. Cubbon[1]

Diabetes 2017;66:2808–2821 | https://doi.org/10.2337/db17-0062

Shc homology 2–containing inositol 5′ phosphatase-2 (SHIP2) is a lipid phosphatase that inhibits insulin signaling downstream of phosphatidylinositol 3-kinase (PI3K); its role in vascular function is poorly understood. To examine its role in endothelial cell (EC) biology, we generated mice with catalytic inactivation of one SHIP2 allele selectively in ECs (ECSHIP2$^{\Delta/+}$). Hyperinsulinemic-euglycemic clamping studies revealed that ECSHIP2$^{\Delta/+}$ was resistant to insulin-stimulated glucose uptake in adipose tissue and skeletal muscle compared with littermate controls. ECs from ECSHIP2$^{\Delta/+}$ mice had increased basal expression and activation of PI3K downstream targets, including Akt and endothelial nitric oxide synthase, although incremental activation by insulin and shear stress was impaired. Insulin-mediated vasodilation was blunted in ECSHIP2$^{\Delta/+}$ mice, as was aortic nitric oxide bioavailability. Acetylcholine-induced vasodilation was also impaired in ECSHIP2$^{\Delta/+}$ mice, which was exaggerated in the presence of a superoxide dismutase/catalase mimetic. Superoxide abundance was elevated in ECSHIP2$^{\Delta/+}$ ECs and was suppressed by PI3K and NADPH oxidase 2 inhibitors. These findings were phenocopied in healthy human ECs after SHIP2 silencing. Our data suggest that endothelial SHIP2 is required to maintain normal systemic glucose homeostasis and prevent oxidative stress-induced endothelial dysfunction.

Insulin resistance is a pathophysiological hallmark of obesity and type 2 diabetes (1). When systemic (2,3), or endothelium-restricted (4,5), insulin resistance leads to an unfavorable imbalance between endothelial cell (EC) generation of the signaling radical nitric oxide (NO) and potentially cytotoxic oxidants, such as superoxide (4,5) and hydrogen peroxide (6). Although the effects of whole-body and cell-specific insulin resistance on EC function are appreciated, the local and systemic consequences of increased insulin signaling in ECs are less well characterized. To address this, we generated mice with endothelium-restricted inhibition of Shc homology 2–containing inositol 5′ phosphatase 2 (SHIP2). SHIP2 is a lipid phosphatase that catalyzes the removal of the 5′ phosphate group from phosphatidylinositol (3–5)-trisphosphate (PI[3,4,5]P_3) (7). PI(3,4,5)P_3 accumulation promotes the activity of signaling molecules, such as Akt; by reducing PI(3,4,5)P_3 accumulation, SHIP2 acts as a negative regulator of insulin-induced Akt signaling (7). Indeed, transgenic mice overexpressing SHIP2 have reduced glucose tolerance and blunted Akt activation in classic insulin target tissues (8).

Three different murine models of SHIP2 loss of function have been generated to examine the role of SHIP2 in insulin signaling. Clément et al. (9) described mice with deletion of *Inppl1* (which encodes SHIP2), although these mice had unplanned deletion of *Phox2a*, a transcription factor involved in normal development. Sleeman et al. (10) studied a second knockout mouse with deletion of *Inppl1*, but intact *Phox2a*; this mouse also had developmental abnormalities. Recently,

[1]Leeds Institute of Cardiovascular and Metabolic Medicine, Leeds Multidisciplinary Cardiovascular Research Centre, University of Leeds, Leeds, U.K.
[2]Laboratory of Functional Genetics, GIGA Research Centre, Université de Liège, Liège, Belgium

Corresponding author: Mark T. Kearney, m.t.kearney@leeds.ac.uk.

Received 12 January 2017 and accepted 4 August 2017.

This article contains Supplementary Data online at http://diabetes.diabetesjournals.org/lookup/suppl/doi:10.2337/db17-0062/-/DC1.

N.T.W. and M.C.G. are joint first authors.

M.C.G. is currently affiliated with the Department of Metabolism and Experimental Therapeutics, Faculty of Medical Sciences, University College London, London, U.K.

© 2017 by the American Diabetes Association. Readers may use this article as long as the work is properly cited, the use is educational and not for profit, and the work is not altered. More information is available at http://www.diabetesjournals.org/content/license.

mice with catalytic inactivation of SHIP2 were generated by inserting Cre-recombinase–specific loxP sites into introns flanking *Inppl1* exons 18–19 (coding the SHIP2 catalytic domain) (11); these mice also had substantial developmental abnormalities, making conclusions regarding insulin signaling challenging.

To improve our understanding of enhanced endothelial insulin signaling, while circumventing the developmental impact of global SHIP2 deletion, we generated mice in which the catalytically inactive SHIP2 described above (11) is restricted to ECs using *Tie2-Cre* (referred to as ECSHIP2$^{\Delta/+}$). We hypothesized that endothelial SHIP2 activity is required to maintain appropriate systemic and vascular responses to insulin.

RESEARCH DESIGN AND METHODS

Generating ECSHIP2$^{\Delta/+}$ Mice

Mice were bred onto a C57BL/6J background for >10 generations in a conventional animal facility with a 12-h light/dark cycle. To examine the effect of chronically increased insulin signaling, male mice that were 10 months of age were used in all experiments, unless stated otherwise, conducted in accordance with accepted standards of humane animal care under UK Home Office project license 40/3523. A catalytically inactive SHIP2 mutant mouse was generated by inserting Cre recombinase–specific loxP sites into intronic regions flanking exons 18–19 of the *Inppl1* gene (11); mice with one floxed allele (SHIP2$^{(18,19)/+}$) were crossed with *Tie2*-Cre mice (The Jackson Laboratory) to produce progeny with germline endothelium–specific SHIP2 inactivation (referred to as ECSHIP2$^{\Delta/+}$). Cre-positive SHIP2$^{+/+}$ littermates were controls in all experiments.

Metabolic Tests

Glucose and insulin tolerance tests were performed by blood sampling after intraperitoneal injection of glucose (1 mg/g) or recombinant human insulin (0.75 unit/kg: ACTRAPID; Novo Nordisk), respectively, as previously described (4,5). Glucose concentrations were determined in whole blood using a portable meter (Roche). Plasma insulin concentrations were determined by ELISA (CrystalChem). Free fatty acids and triglycerides were measured in fasting plasma using colorimetric assays (Abcam) (12).

In Vivo Hyperinsulinemic-Euglycemic Clamp Studies

In vivo euglycemic insulin clamps were performed at the Mouse Metabolic Phenotyping Center at Vanderbilt University (Nashville, TN), as previously described (13). These use tracer techniques to assess the following: *1*) whole-body insulin sensitivity; *2*) insulin suppression of endogenous (i.e., hepatic) glucose production; and *3*) rates of individual tissue glucose uptake.

Experimental Protocol

Mice were maintained on a chow diet (Diet 7012; Teklad). Catheters were implanted in a carotid artery for blood sampling and in a jugular vein for infusions 5 days before the study. On the morning of each study, food was removed and clamps were initiated after a 5-h fast. One hundred twenty minutes (t = −120 min) prior to initiation of the clamps, animals received a bolus (1.5 μCi) followed by a continuous (0.075 μCi/min) infusion of [3-^{3}H]glucose. Baseline blood or plasma parameters were determined in blood samples collected at −10 and 0 min. At t = 0, an insulin infusion (4 mU/kg/min) was started, the infusion rate of [3-^{3}H]glucose was increased (0.15 μCi/min), and a constant infusion of heparinized saline washed with erythrocytes from donor animals (5.5 μL/min) were administered to prevent a fall in hematocrit. These infusions were continued for the duration of the clamp (145 min). The blood glucose concentration was clamped at ~100–110 mg/dL using a variable glucose infusion rate (GIR). Blood glucose was monitored every 10 min to validate clamping, and the GIR was adjusted accordingly. Blood was taken at between 80 and 120 min for the determination of [3-^{3}H]glucose. Clamp insulin was determined at t = 120 and 145 min. At 120 min, 13 μCi of 2[^{14}C]deoxyglucose ([^{14}C]2DG) was administered as an intravenous bolus. Blood was taken at between 122 and 145 min for the determination of [^{14}C]2DG. After the last sample, mice were euthanized and tissue samples were collected.

Plasma and Muscle Sample Analysis

Immunoreactive insulin was assayed with a rat radioimmunoassay kit (Millipore). To measure plasma 3-[^{3}H]-D-glucose, the sample was deproteinized with barium hydroxide ($Ba[OH]_2$) and zinc sulfate ($ZnSO_4$), dried, and radioactivity determined using liquid scintillation counting. Excised soleus, gastrocnemius, superficial vastus lateralis, and gonadal adipose tissue were deproteinized with percholoric acid and then neutralized to approximately pH 7.5. A portion of the extract was counted ([2-^{14}C]DG and [2-^{14}C]DG-G-phosphate ([2-^{14}C]DGP) and a portion treated with $Ba(OH)_2$ and $ZnSO_4$ and the supernatant was counted ([2-^{14}C]DG). Both [2-^{14}C]DG and [2-^{14}C]DGP radioactivity levels were determined using liquid scintillation counting.

Studies of Vasomotor Function in Aortic Rings

Vasomotor function was assessed ex vivo in aortic rings as previously described (2–5). Rings were mounted in an organ bath containing Krebs-Henseleit buffer (composition [in mmol/L]: NaCl 119, KCl 4.7, KH_2PO_4 1.18, $NaHCO_3$ 25, $MgSO_4$ 1.19, $CaCl_2$ 2.5, and glucose 11.0) and gassed with 95% O_2/5% CO_2. Rings were equilibrated at a resting tension of 3*g* for 45 min. A cumulative dose response to the constrictor phenylephrine (PE) (1 nmol/L to 10 μmol/L) was performed. Vasodilation to insulin was assessed with incremental doses of ACTRAPID insulin (0.1–1,000 mU/mL) in aortic segments preconstricted maximally with PE. Relaxation responses to cumulative addition of acetylcholine (1 nmol/L to 10 μmol/L) and sodium nitroprusside (0.1 nmol/L to 1 μmol/L) were performed. The effects of MnTmPyP (10 μmol/L for 30 min; Calbiochem) on aortic relaxation were examined, as previously reported (2). Relaxation responses are expressed as the percentage decrement in preconstricted tension. Bioavailable NO in aortic segments

subject to isometric tension was measured by recording the increase in tension elicited by N^G-monomethyl-L-arginine (L-NMMA) (0.1 mmol/L) in aortic segments maximally preconstricted with PE.

Amplex Red Assay for Hydrogen Peroxide in Aorta

H_2O_2 was measured using an Amplex Red Hydrogen Peroxide/Peroxidase Assay Kit (Thermo Fisher Scientific), according to the manufacturer protocol. Freshly harvested aortae were collected into modified Krebs-HEPES buffer, containing 20 mmol/L HEPES, 119 mmol/L NaCl, 4.6 mmol/L KCl, 1 mmol/L $MgSO_40.7H_2O$, 0.15 mmol/L Na_2HPO_4, 0.4 mmol/L KH_2PO_4, 5 mmol/L $NaHCO_3$, 1.2 mmol/L $CaCl_2$, and 5.5 mmol/L glucose, pH 7.4. Aortas were cleaned of adipose tissue and divided into 2-mm rings. Rings were incubated in 50 μL of modified Krebs-HEPES buffer with half also receiving 1,250 units/mL catalase (free from thymol) for 1 h at 37°C. Fifty microliters of freshly prepared 100 μmol/L Amplex Red reagent with 0.2 units/mL horseradish peroxidase was added to samples and incubated for 1 h at 37°C, protected from light. Rings were removed from the samples and fluorescence measured on a Varioskan plate reader (Thermo Fisher Scientific) (excitation 530 nm, emission 590 nm). The mean reading with catalase was subtracted from the mean without catalase, and this value was plotted on a simultaneously prepared H_2O_2 standard curve. Dry tissue mass was used for normalization (12).

Pulmonary EC Isolation and Culture

Primary ECs were isolated from lungs by immunoselection with CD146 antibody–coated magnetic beads as previously reported (4,14) and cultured in 2 mL of EGM-2-MV (Lonza) supplemented with 5% FCS until confluent. These express a range of endothelial markers including endothelial NO synthase (eNOS), *Tie2*, and CD102 protein (4,14).

SHIP2 Activity Assay

SHIP2 activity was measured using the 5′PtdIns(3,4,5)P_3 Phosphatase Activity Fluorescent Polarization Assay (Echelon Biosciences) according to the manufacturer instructions, using a Polarstar Optima plate reader (BMG Labtech) with excitation at 550 nm and measuring polarized emission at 580 nm.

NO Synthase Activity in ECs

Active eNOS produces NO and L-citrulline from L-arginine in a stoichiometric reaction. Insulin-stimulated eNOS activity in ECs was determined by the conversion of [^{14}C]-L-arginine to [^{14}C]-L-citrulline as previously described (14,15). ECs (1×10^6) were incubated at 37°C for 20 min in HEPES buffer pH 7.4 as follows (in mmol/L): 10 HEPES, 145 NaCl, 5 KCl, 1 MgSO4, 10 glucose, and 1.5 $CaCl_2$ containing 0.25% BSA. 0.5 μCi/mL [^{14}C]-L-arginine was then added for 5 min prior to stimulation with insulin (100 nmol/L) for 15 min before the reaction was stopped with cold PBS containing 5 mmol/L unlabeled L-arginine and 4 mmol/L EDTA, after which cells were denatured in 95% ethanol. After evaporation, the pellet was dissolved in 20 mmol/L HEPES-Na^+ (pH 5.5) and applied to a well-equilibrated Dowex (Na^+ form) column. The eluate [^{14}C]-L-citrulline content was quantified by liquid scintillation and normalized against total protein mass.

Exposure of ECs to Flow-Mediated Shear Stress

Pulmonary ECs were seeded onto fibronectin-coated 6-well plates. Confluent monolayers were placed onto an orbital rotating platform (Grant Instruments) inside an incubator (16). The radius of orbit of the orbital shaker was 10 mm, and the rotation rate was set to 210 rpm for 10 min, generating a shear force of 12 dyne/cm^2.

Lucigenin Enhanced Chemiluminescence

We used lucigenin (5 μmol/L), enhanced chemiluminescence to measure NADPH-dependent superoxide production in pulmonary ECs, as previously described (12). All experiments were performed in triplicate. Pulmonary ECs were suspended in PBS containing 5% FCS, 0.5% BSA, and 50 μmol/L Gp91ds-tat (GenScript) or scrambled ds-tat peptide (GenScript) and incubated at 37°C for 30 min. Luminescence was measured upon the addition of a nonredox cycling concentration of lucigenin (5 μmol/L) and NADPH (100 μmol/L) using an autodispenser (Varioskan; Thermo Fisher Scientific).

Cell Lysis, Immunoblotting, and Immunoprecipitation

Pulmonary ECs were lysed in extraction buffer containing the following (in mmol/L, unless otherwise specified): 50 HEPES, 120 NaCl, 1 $MgCl_2$, 1 $CaCl_2$, 10 NaP_2O_7, 20 NaF, 1 EDTA, 10% glycerol, 1% NP-40, 2 sodium orthovanadate, 0.5 μg/mL leupeptin, 0.2 phenylmethylsulfonyl fluoride, and 0.5 μg/mL aprotinin. Cell extracts were sonicated in an ice bath and centrifuged for 15 min before protein measurement using the BCA Assay (Thermo Fisher Scientific). Equal amounts of protein were resolved on SDS-polyacrylamide gels (Thermo Fisher Scientific) and transferred to polyvinylidine difluoride membranes. Immunoblotting was carried out with primary antibodies produced by Cell Signaling Technologies, except for the following: mouse NADPH oxidase 2 (NOX2), mouse insulin receptor, mouse insulin receptor substrate (IRS) 1, mouse IRS2, and human SHIP2 (Abcam); human NOX2 and β-actin (Santa Cruz Biotechnology); mouse SHIP2 (gift from Stéphane Schurmans, Université de Liège, Liège, Belgium). Blots were incubated with appropriate peroxidase-conjugated secondary antibodies and developed with enhanced chemiluminescence (Millipore).

Lentiviral Knockdown of SHIP2 in Human Umbilical Vein ECs

Knockdown of SHIP2 in human umbilical vein ECs (HUVECs) (PromoCell, Heidelberg, Germany) was performed with short hairpin RNA (shRNA) transduction using a lentivirus vector (catalog #SHCLNV-NM001567; Sigma-Aldrich) as previously described (17). HUVECs were transduced with a multiplicity of infection of 10 and incubated at 37°C for 4 days prior to analysis. Control cells were transduced with a green fluorescent protein–targeting control shRNA lentivirus (catalog #SHC002H; Sigma-Aldrich).

Gene Expression

mRNA was isolated using TRIzol (Thermo Fisher Scientific), and SHIP2 mRNA was quantified using SYBR-Green–based real-time quantitative PCR using (ABI Prism 7900HT; Applied Biosystems) (4). Primer details are as follows: truncated SHIP2 forward 5′-ACC-TTA-ACT-ACC-GCT-TAG-ACA-TGG-A; truncated SHIP2 reverse 5′-ATC-AGT-GCA-ACT-AAA-TCG-AAG-GAA; nontruncated region of SHIP2 forward 5′-AAG-ACT-ACT-CGG-CGG-AAC-CA; nontruncated region of SHIP2 reverse 5′-TGC-CGA-TCA-CCC-AAC-GA; β-actin forward 5′-CGT-GAA-AAG-ATG-ACC-CAG-ATC-A; and β-actin reverse 5′-TGG-TAC-GAC-CAG-AGG-CAT-ACA-G. As published (12), RNA was also isolated from purified $CD11b^+$ myeloid cells to define truncated SHIP2 expression. TaqMan (Thermo Fisher Scientific) assays were used to measure the expression of interleukin (IL)-1β (catalog #mm00434228_m1), IL-6 (catalog #mm00446190_m1), and tumor necrosis factor-α (TNF-α) (catalog #mm00443258_m1) in gastrocnemius muscle and epididymal adipose tissue.

Flow Cytometry

Heparinized whole blood underwent erythrocyte lysis (Pharmalyse; BD Biosciences) prior to isolation of peripheral blood mononuclear cells by centrifugation. After blocking with CD16/32 Fc block (BD Biosciences), cells were stained with anti-CD45-VioBlue, anti-CD11b-FITC, and anti-Ly6G-PE (all from Miltenyi Biotec); and Ly6C-APC (eBioscience). Paired samples were prepared with corresponding isotype-specific controls. Flow cytometry (LSRFortessa; BD Biosciences) was performed to define the following subsets: total leukocytes ($CD45^+$); myeloid cells ($CD45^+CD11b^+$); monocytes ($CD45^+CD11b^+Ly6G^-Ly6C^+$); neutrophils ($CD45^+CD11b^+Ly6G^{hi-}Ly6C^{hi}$); "inflammatory" monocytes ($CD45^+CD11b^+Ly6G^-Ly6C^{hi}$); "patrolling" monocytes ($CD45^+CD11b^+Ly6G^-Ly6C^{lo}$). All populations are expressed as the number of cells per milliliter blood.

Cytokine ELISA

Serum IL-6 and TNF-α were measured with commercially available ELISAs according to manufacturer instructions (Abcam) (12).

Histology

Adipose Inflammation

Epididymal fat fixed in 4% paraformaldehyde was embedded in paraffin blocks and 5-μm sections stained with Sirius Red (Sigma-Aldrich) to demarcate collagen deposition, which is a feature of inflammation (18). The percentage of the Sirius Red staining area was calculated with ImageJ (National Institutes of Health).

Adipose Vascularity

Epididymal fat fixed in 1% paraformaldehyde then stained with LipidTOX Green (Thermo Fisher Scientific) and isolectin-B4-Alexa647 (Thermo Fisher Scientific) was whole mounted in chamber slides and imaged with a confocal microscope (catalog #LSM880; Zeiss). The vascular (isolectin-B4) percentage area was calculated in thresholded 4-μm maximum intensity projections using ImageJ (National Institutes of Health).

Skeletal Muscle Vascularity

Gastrocnemius muscle fixed in 4% paraformaldehyde was embedded in Tissue-Tek O.C.T. compound (Sakura) and snap frozen. The 5-μm cryosections were stained with isolectin-B4-Alexa Fluor 647 (Thermo Fisher Scientific) and DAPI (Southern Biotech) then imaged with a confocal microscope (catalog #LSM880; Zeiss). The percentage of vascular area (isolectin-B4) was calculated in thresholded 2-μm maximum intensity projections using ImageJ (National Institutes of Health).

Statistics

Results are expressed as the mean (SEM). Comparisons within groups were made using paired Student *t* tests and between groups using unpaired Student *t* tests or repeated-measures ANOVA, as appropriate. $P < 0.05$ was considered to be statistically significant.

RESULTS

Basic Characterization of Mice With Endothelium-Specific Inactivation of SHIP2

To examine the effect of reducing the restraining role of SHIP2 on insulin action specifically in the endothelium, we generated mice with Tie2-Cre–mediated catalytic inactivation of one SHIP2 allele ($ECSHIP2^{\Delta/+}$). $ECSHIP2^{\Delta/+}$ mice were born with the same frequency as control littermates. There was no difference in gross appearance (Fig. 1*A*), organ weight (Fig. 1*B*), or body length (Fig. 1*C*) when comparing $ECSHIP2^{\Delta/+}$ and control mice, although 10-month-old $ECSHIP2^{\Delta/+}$ mice were slightly heavier (Fig. 1*D*). We quantified truncated SHIP2 mRNA in organs with differing vascularity; as expected, $SHIP2^{\Delta 18-19}$ mRNA was only detectable above nonspecific fluorescence in $ECSHIP2^{\Delta/+}$ organs, not control organs (Fig. 1*E*). $SHIP2^{\Delta 18-19}$ mRNA was also undetectable in non-ECs from $ECSHIP2^{\Delta/+}$ lungs (Fig. 1*F*) but was just detectable in $CD11b^+$ myeloid cells (>3,000-fold lower than $ECSHIP2^{\Delta/+}$ pulmonary EC, and ~5-fold above nonspecific fluorescence) (Supplementary Fig. 1*A*). Endothelial SHIP2 protein expression was mildly reduced in $ECSHIP2^{\Delta/+}$ mice (Fig. 1*G*), whereas SHIP2 activity was substantially reduced (Fig. 1*H*), which is in keeping with targeted catalytic domain deletion, as shown previously in work using $SHIP2^{(18,19)/+}$ mice (11).

$ECSHIP2^{\Delta/+}$ Mice Do Not Exhibit a Proinflammatory State

As very low-level expression of truncated SHIP2 was found in myeloid cells, we conducted a detailed assessment of systemic and tissue-specific inflammation. Flow cytometry revealed no difference in circulating leukocyte populations (Supplementary Fig. 1*B*), and leukocyte SHIP2 activity was comparable in $ECSHIP2^{\Delta/+}$ and control littermates (Supplementary Fig. 1*C*). $ECSHIP2^{\Delta/+}$ mice had normal serum levels of TNF-α and IL-6 (Supplementary Fig. 1*D* and *E*) along with normal expression of TNF-α, IL-1β, and IL-6 in white adipose tissue and skeletal muscle (Supplementary Fig. 1*F*). We found no evidence of altered adipose tissue inflammation using Sirius Red collagen staining (Supplementary Fig. 1*G*).

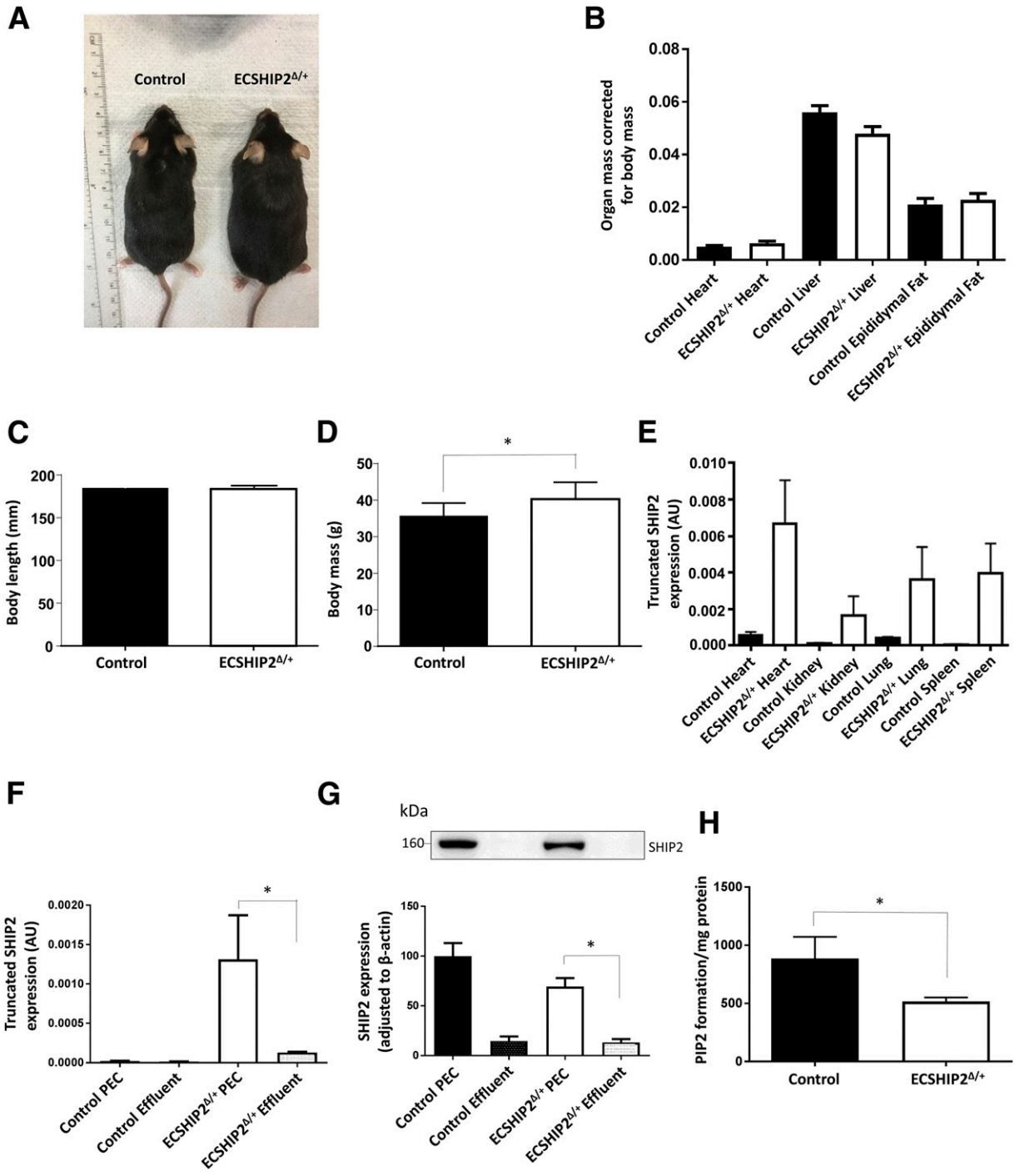

Figure 1—Basic characterization of ECSHIP2$^{\Delta/+}$ mice. Compared with control Cre^{+} littermate controls, no difference was seen in the gross development of ECSHIP2$^{\Delta/+}$ mice (*A*); ECSHIP2$^{\Delta/+}$ organ weights were comparable ($n \geq 7$) (*B*); the nose-to-tail length of ECSHIP2$^{\Delta/+}$ mice was similar ($n \geq 4$) (*C*); ECSHIP2$^{\Delta/+}$ mice were slightly heavier ($n \geq 6$) (*D*); truncated SHIP2 mRNA was detectable in organs from ECSHIP2$^{\Delta/+}$ mice, but not controls ($n = 3$) (*E*); truncated SHIP2 mRNA was detectable only in ECs from ECSHIP2$^{\Delta/+}$ lungs and not in the non-EC fraction ($n = 3$) (*F*); SHIP2 protein expression (representative Western blot shown above the panel) was mildly reduced in ECs from ECSHIP2$^{\Delta/+}$ mice ($n \geq 5$) (*G*); and SHIP2 activity was substantially reduced in ECs from ECSHIP2$^{\Delta/+}$ mice ($n \geq 9$) (*H*). AU, arbitrary units; PEC, pulmonary EC. *$P < 0.05$.

ECSHIP2$^{\Delta/+}$ Mice Have Reduced Glucose Tolerance and Insulin Sensitivity

Compared with control littermates, ECSHIP2$^{\Delta/+}$ mice had higher fasting glucose concentrations (Fig. 2*A*), similar fasting insulin concentrations (Fig. 2*B*), and higher HOMA-insulin resistance (Fig. 2*C*). ECSHIP2$^{\Delta/+}$ mice had delayed normalization in capillary glucose during glucose tolerance testing (Fig. 2*D*), but insulin tolerance test results were similar to

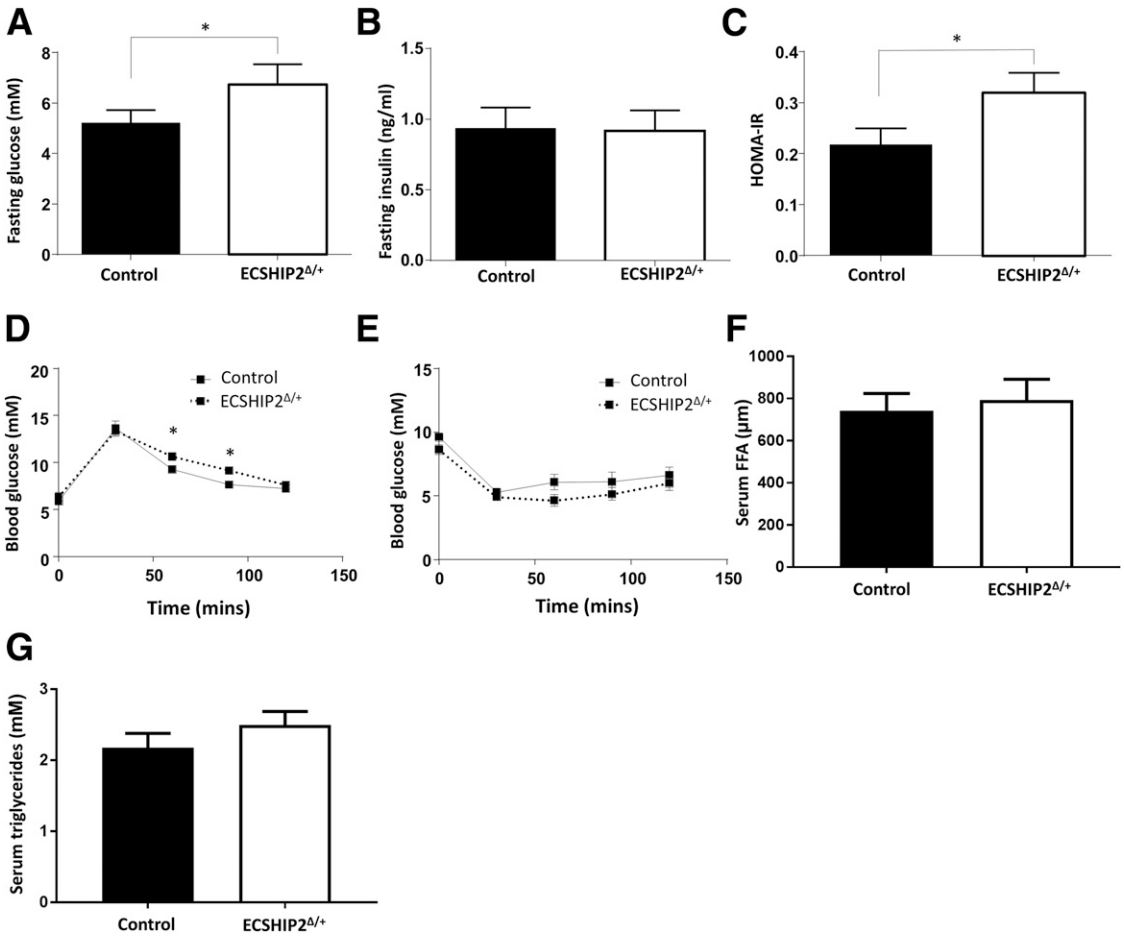

Figure 2—Abnormal glucose homeostasis in ECSHIP2$^{\Delta/+}$ mice. *A*: Fasting glucose was increased in ECSHIP2$^{\Delta/+}$ mice ($n = 7$). *B*: Fasting insulin in ECSHIP2$^{\Delta/+}$ mice was comparable to that of controls ($n \geq 6$). *C*: HOMA-insulin resistance (IR) was increased in ECSHIP2$^{\Delta/+}$ mice ($n \geq 12$). *D*: Glucose tolerance was impaired in ECSHIP2$^{\Delta/+}$ mice ($n \geq 8$). *E*: Insulin tolerance testing was similar in ECSHIP2$^{\Delta/+}$ mice vs. controls ($n \geq 8$). *F*: Serum free fatty acid (FFA) levels were similar in ECSHIP2$^{\Delta/+}$ mice vs. controls ($n \geq 6$). *G*: Serum triglyceride levels were similar in ECSHIP2$^{\Delta/+}$ mice vs. controls ($n \geq 6$). *$P < 0.05$.

those in control littermates (Fig. 2*E*). Levels of serum free fatty acids (Fig. 2*F*) and triglycerides (Fig. 2*G*) were not altered in ECSHIP2$^{\Delta/+}$ mice. In hyperinsulinemic-euglycemic clamp studies, ECSHIP2$^{\Delta/+}$ mice required ~25% less glucose to maintain euglycemia than controls (Fig. 3*A*). In tracer studies, glucose uptake into adipose tissue and skeletal muscle was reduced (Fig. 3*B*), whereas hepatic glucose output was no different between ECSHIP2$^{\Delta/+}$ mice and controls (Fig. 3*C* and *D*).

ECs From ECSHIP2$^{\Delta/+}$ Mice Have Increased Basal Activation of Signaling Molecules Downstream of Phosphatidylinositol 3-Kinase, Although Incremental Activation by Insulin and Shear Stress Is Impaired

In the endothelium, phosphatidylinositol 3-kinase (PI3K) transduces insulin signaling by catalyzing the addition of a phosphate group to the 3′ position of inositol rings, generating 3′-phosphoinositides, including $PI(3,4,5)P_3$, which by activating phosphoinositide-dependent kinase-1 (PDK1) activates the serine/threonine kinase Akt/PKB (19). Akt activates downstream signaling molecules including eNOS (20). ECSHIP2$^{\Delta/+}$ had increased basal expression of total PDK1 and phosphorylated (p) PDK1, total Akt, and T308 pAkt, total eNOS, and S1177 peNOS, Rictor (which phosphorylates Akt at S473), and pRictor (Fig. 4*A*). Importantly, 6-week-old ECSHIP2$^{\Delta/+}$ mice had normal endothelial total Akt, Rictor, and eNOS expression and normal adipose tissue and skeletal muscle vascularity (Supplementary Fig. 2), suggesting that adulthood signaling abnormalities do not reflect persistent developmental abnormalities. ECSHIP2$^{\Delta/+}$ had comparable insulin-stimulated induction of Akt S473 phosphorylation but diminished downstream induction of eNOS S1177 phosphorylation compared with controls (Fig. 4*B*). PI3K/Akt also mediate shear-induced eNOS activation in ECs; ECSHIP2$^{\Delta/+}$ ECs exhibited no increase in the phosphorylation of Akt S473 or eNOS S1177 in response to shear stress (Fig. 4*C*). Notably, we found no significant differences in basal or insulin-stimulated phosphorylation of the insulin receptor or insulin receptor substrates 1/2 (Supplementary Fig. 3).

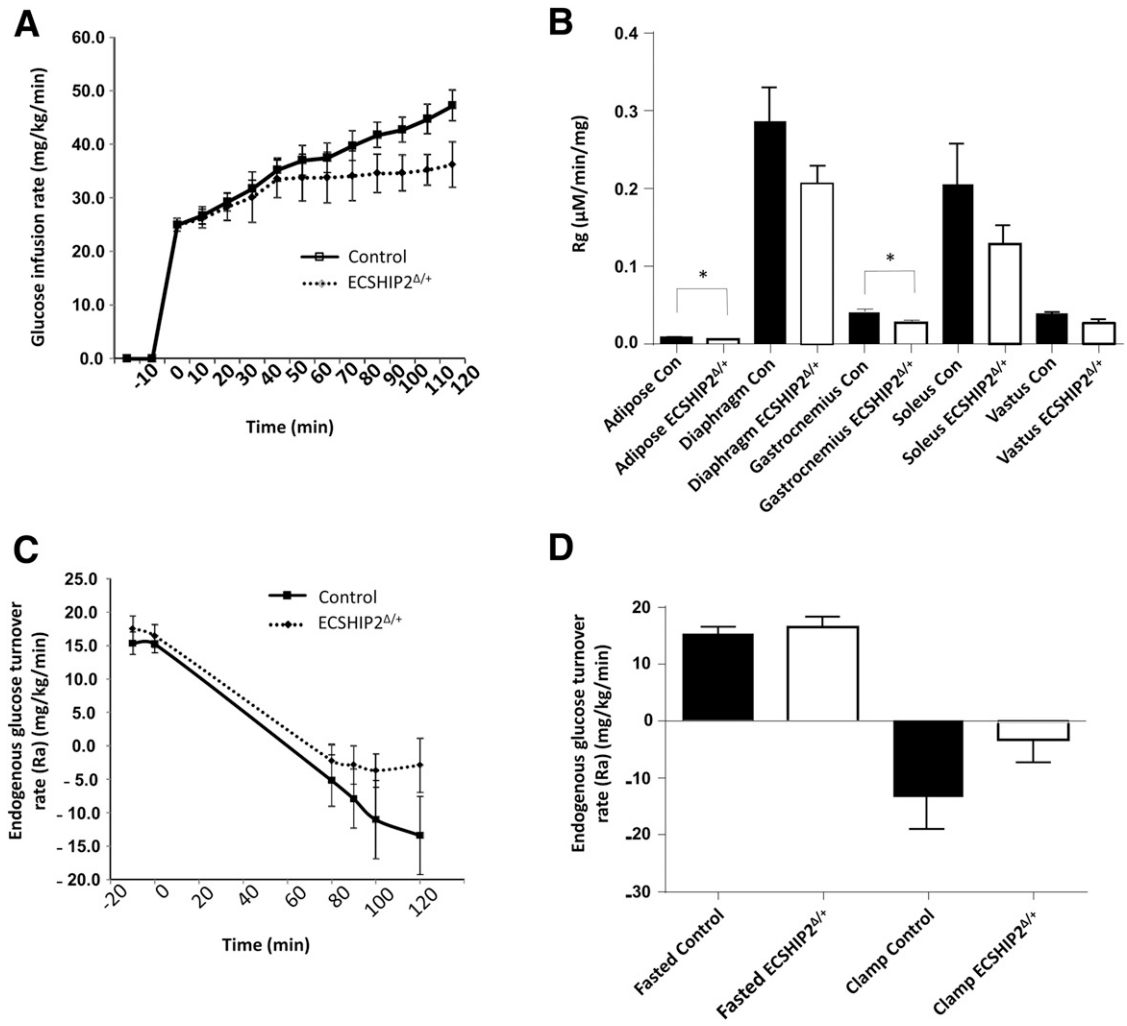

Figure 3—Insulin resistance in ECSHIP2$^{\Delta/+}$ mice during hyperinsulinemic-euglycemic clamping. *A*: Reduced insulin infusion rate (i.e., GIR) in ECSHIP2$^{\Delta/+}$ indicative of insulin resistance. *B*: Blunted glucose uptake in muscle and fat from ECSHIP2$^{\Delta/+}$ mice. *C* and *D*: Comparable hepatic glucose output in ECSHIP2$^{\Delta/+}$ mice vs. controls ($n \geq 4$ for all experiments). Con, control; Rg, insulin-mediated glucose metabolic index. *$P < 0.05$.

ECSHIP2$^{\Delta/+}$ Mice Have Blunted Acetylcholine- and Insulin-Mediated Aortic Vasodilation Associated With Vascular Oxidative Stress

Ex vivo aortic vasomotor responses were studied in an organ bath apparatus. Consistent with our findings in ECs, ECSHIP2$^{\Delta/+}$ mice had blunted insulin-mediated vasodilation (Fig. 5*A*). ECSHIP2$^{\Delta/+}$ mice exhibited significantly less constriction to the nonselective NOS inhibitor L-NMMA (Fig. 5*B–D*), which is indicative of reduced NO biogenesis in response to isometric tension. There was subtle impairment of acetylcholine-induced relaxation in ECSHIP2$^{\Delta/+}$ mice (Fig. 5*E*), but sodium nitroprusside responses were comparable to those of controls (Fig. 5*F*). To explore whether vasodilating oxidants were masking more substantial impairment of acetylcholine-mediated vasodilation in ECSHIP2$^{\Delta/+}$ mice, we repeated acetylcholine relaxation studies in the presence of the superoxide dismutase/catalase mimetic MnTmPyP. MnTmPyP reduced acetylcholine-mediated aortic relaxation in ECSHIP2$^{\Delta/+}$ and control vessels, but the extent of inhibition was significantly greater in ECSHIP2$^{\Delta/+}$ vessels (Fig. 5*G–K*). Hydrogen peroxide, the more stable product of superoxide dismutation, was also elevated in ECSHIP2$^{\Delta/+}$ aortae (Fig. 5*L*). In isolated lung ECs, superoxide abundance was increased, as assessed by lucigenin-enhanced chemiluminescence and with dihydroethidium fluorescence (Fig. 6*A*). Superoxide is generated by many enzymes, and we have shown that Nox2 NADPH oxidase is a critical pathophysiological source of superoxide in models of global insulin resistance (4,5). In ECSHIP2$^{\Delta/+}$ ECs, Nox2 protein expression was increased (Fig. 6*B*). Moreover, superoxide abundance was normalized with the Nox2-specific inhibitor Gp91ds-tat (Fig. 6*C*) and the PI3K inhibitors Wortmannin and LY294002 (Fig. 6*D*). Oxidative stress is often associated with reduced eNOS activity, and this was confirmed in ECSHIP2$^{\Delta/+}$ ECs treated with insulin (Fig. 6*E*).

SHIP2 Knockdown in Human ECs Phenocopies the Signaling Abnormalities of ECSHIP2$^{\Delta/+}$

Next, we sought to validate and generalize the mechanistic data from our murine model, using a complementary system

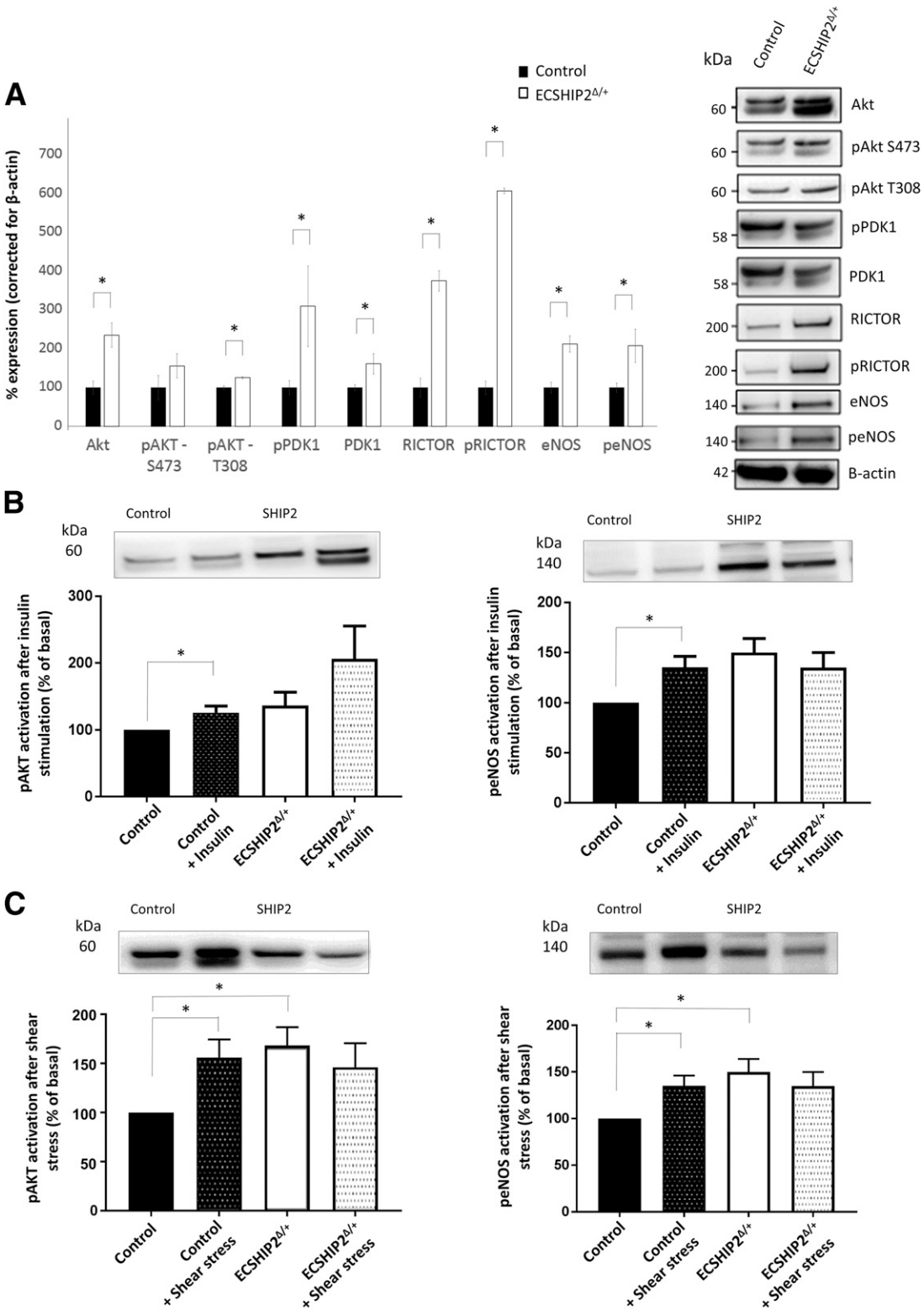

Figure 4—EC insulin signaling and mechanical shear stress signaling are impaired in ECSHIP2$^{\Delta/+}$ mice. *A*: The basal abundance of Akt, pAkt T308, PDK1, pPDK1, Rictor, pRictor, eNOS, and peNOS S1177 were increased in ECSHIP2$^{\Delta/+}$ ECs exposed to standard culture media ($n \geq 4$). *B*: Insulin-stimulated (150 nm for 10 min) phosphorylation of eNOS, but not Akt, was impaired in ECSHIP2$^{\Delta/+}$ ECs ($n \geq 6$). *C*: Shear stress induction (10 min) of Akt and eNOS phosphorylation was impaired in ECSHIP2$^{\Delta/+}$ ECs ($n \geq 6$). Representative Western blots are shown above all panels. *$P < 0.05$.

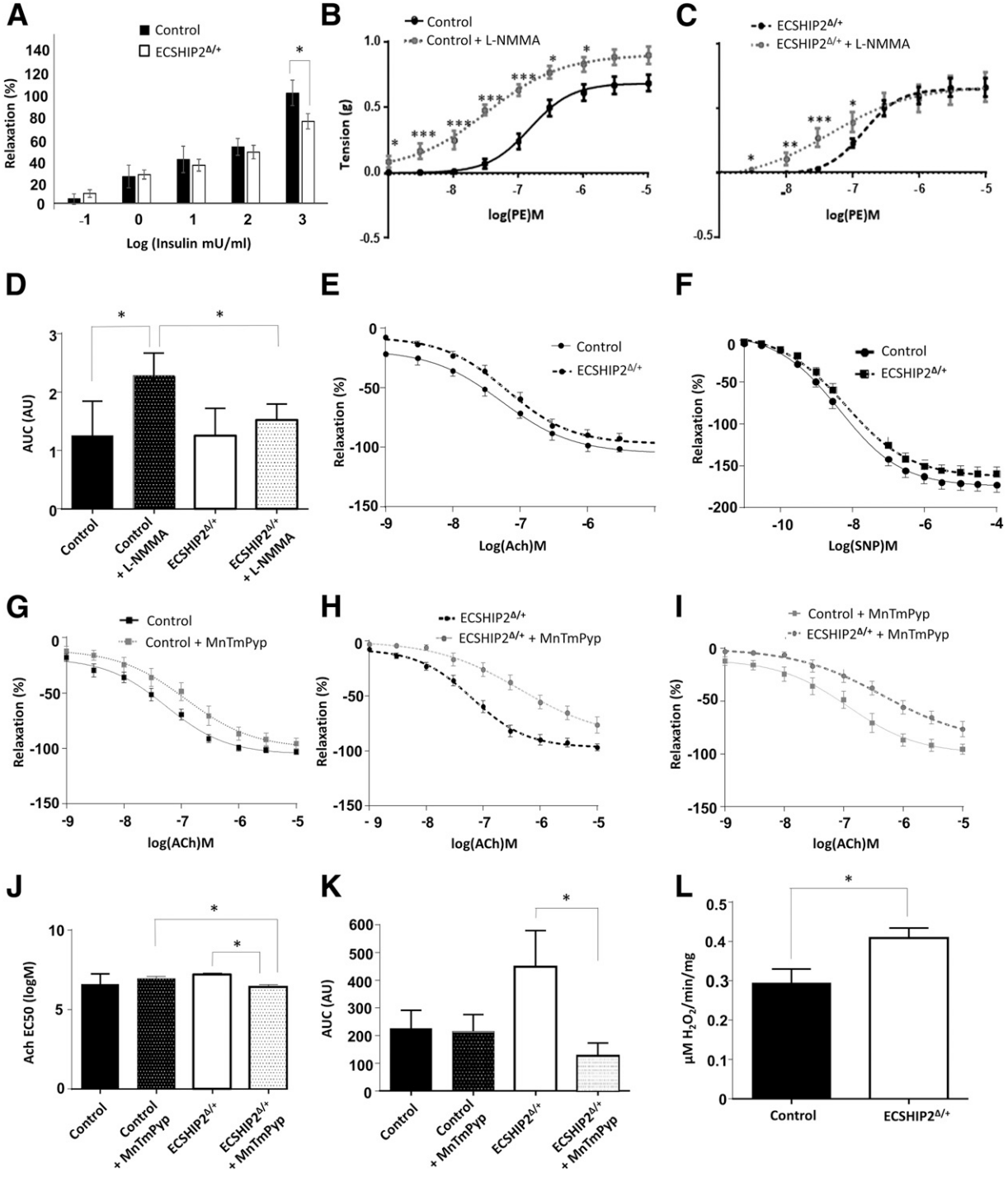

Figure 5—Impaired aortic vasodilation in ECSHIP2$^{\Delta/+}$ mice is associated with oxidative stress and reduced NO bioavailability. *A*: Reduced insulin-mediated aortic relaxation in ECSHIP2$^{\Delta/+}$ mice ($n \geq 4$). *B–D*: Reduced L-NMMA–induced vasoconstriction in ECSHIP2$^{\Delta/+}$ mice indicative of reduced NO bioavailability ($n \geq 3$). *E* and *F*: Subtle impairment of acetylcholine-mediated vasodilation in aortae from ECSHIP2$^{\Delta/+}$ mice ($n \geq 8$). *F*: No difference in sodium nitroprusside (SNP)–mediated vasodilation in aortic rings from ECSHIP2$^{\Delta/+}$ mice ($n \geq 3$). *G–K*: MnTmPyP blunts acetylcholine-mediated vasodilation in aortae from ECSHIP2$^{\Delta/+}$ mice and controls, but the reduction in acetylcholine-mediated vasodilation is greater in ECSHIP2$^{\Delta/+}$ mice ($n \geq 4$). *L*: Increased aortic hydrogen peroxide generation in ECSHIP2$^{\Delta/+}$ mice ($n \geq 4$). ACh, acetylcholine; AU, arbitrary units; AUC, area under the curve; M, molar. $^{*}P < 0.05$; $^{**}P < 0.005$; $^{***}P < 0.005$.

in human ECs. We used lentiviral vectors to express SHIP2-targeting shRNA, or a nontargeting control shRNA, to knock down SHIP2 in HUVECs, achieving ~75% reduction in SHIP2 protein versus that in controls (Fig. 7*A*). As seen in ECSHIP2$^{\Delta/+}$ ECs, the knockdown of SHIP2 reduced SHIP2 activity (Fig. 7*B*) and enhanced superoxide concentrations (Fig. 7*C*). We examined potential sources of superoxide and again demonstrated increased Nox2 NADPH oxidase expression

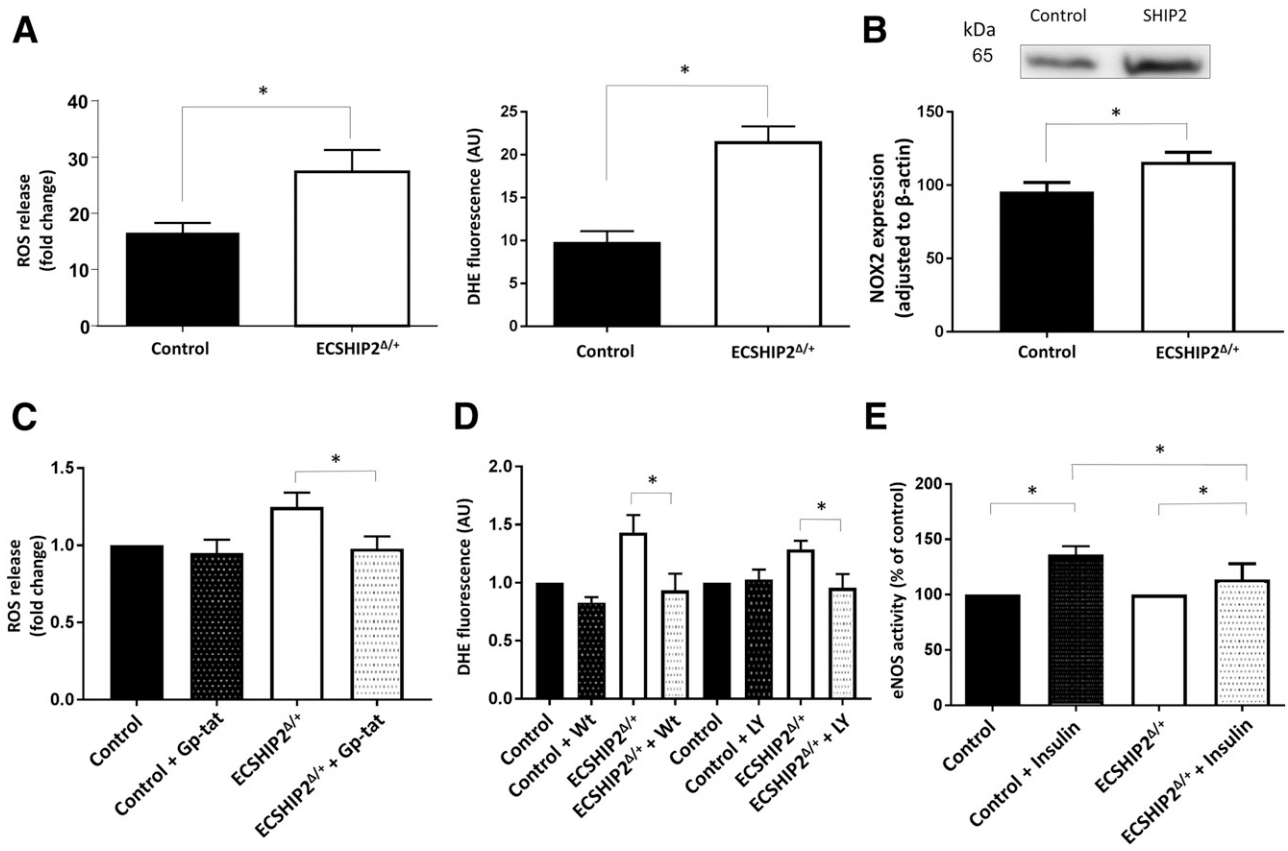

Figure 6—ECSHIP2$^{\Delta/+}$ ECs exhibit PI3K- and Nox2-dependent oxidative stress and reduced NO generation. *A*: Increased superoxide generation in ECSHIP2$^{\Delta/+}$ mice, measured with lucigenin-enhanced chemiluminescence (left: $n \geq 10$) and dihydroethidium (DHE) fluorescence (right: $n \geq 3$). *B*: Increased Nox2 NADPH oxidase protein (representative Western blot shown above the panel) in ECSHIP2$^{\Delta/+}$ mice ($n \geq 9$). *C*: Increased superoxide abundance in ECSHIP2$^{\Delta/+}$ mice is normalized by Gp91ds-tat ($n \geq 4$). *D*: Increased superoxide abundance in ECSHIP2$^{\Delta/+}$ mice is normalized by the PI3K inhibitors Wortmannin and LY294002 ($n \geq 4$). *E*: Insulin-stimulated NO production is impaired in ECs from ECSHIP2$^{\Delta/+}$ mice ($n \geq 5$). ROS, reactive oxygen species. AU, arbitrary units; GP-tat, Gp91ds-tat NADPH oxidase 2 inhibitor; WT, Wortmannin; LY, LY294002 PI3K inhibitor. *$P < 0.05$.

(Fig. 7*D*); moreover, the excess superoxide seen in SHIP2-deficient cells was inhibited by Gp91ds-tat (Fig. 7*E* and *F*). Furthermore, in SHIP2 knockdown HUVECs, S473 pAkt and S1177 peNOS was more abundant (Fig. 7*G*), and superoxide abundance was reduced by the PI3K inhibitors Wortmannin and LY294002 (Fig. 7*H*). These data imply that increased PI3K signaling drives Nox2-dependent superoxide production in the context of human EC SHIP2 knockdown.

DISCUSSION

We provide a number of novel findings pertaining to the understanding of endothelial SHIP2 signaling and metabolic disease: *1*) EC-specific reduction of SHIP2 activity is not associated with developmental defects; *2*) mice with EC-specific reduction of SHIP2 activity develop insulin resistance in skeletal muscle and fat, which is not associated with evidence of inflammation; *3*) EC-specific reduction of SHIP2 activity is associated with endothelial dysfunction, excess superoxide abundance, and reduced NO bioavailability; and *4*) oxidative stress associated with SHIP2 knockdown in murine and human ECs is caused by excessive PI3K signaling and is Nox2 NADPH oxidase dependent. Our data emphasize the detrimental impact of increased PI3K/Akt signaling on EC function and confirm the key role of SHIP2 in maintaining vascular homeostasis. In particular, they reveal that increased basal PI3K/Akt signal transduction in ECs is associated with Nox2-mediated vascular oxidative stress and paradoxical systemic insulin resistance due to impaired adipose tissue and skeletal muscle glucose uptake. Therefore, although hyperinsulinemia is an adaptive response to hyperglycemia, when sustained this may have detrimental effects on vascular function and glucose uptake in key metabolic tissues; this raises important questions about the long-term risks of therapies that induce sustained insulin signaling.

SHIP2, Insulin Signaling, PI3K, and Akt

The ligand-bound insulin receptor phosphorylates tyrosine residues on downstream substrates, activating PI3K, which catalyzes phosphorylation of the 3′ position of inositol rings, generating 3′ phosphoinositides including PI(3,4,5)P_3 (21). PI(3,4,5)P_3 recruits the serine/threonine kinase Akt to the cell membrane, facilitating its activation and allowing the phosphorylation of downstream effectors, including eNOS (19). Short-term in vivo studies have examined the effect of

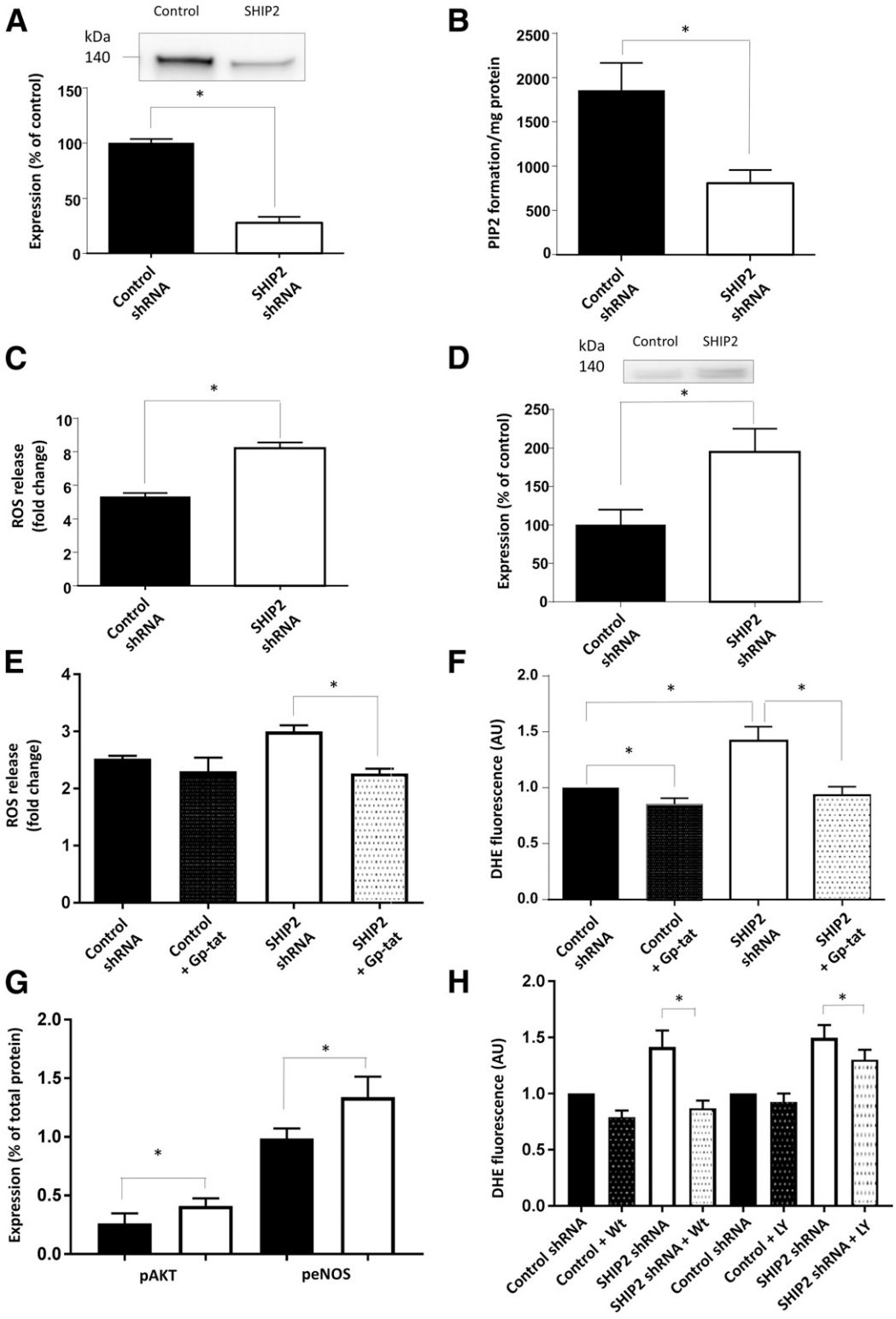

Figure 7—shRNA knockdown of SHIP2 in HUVECs recapitulates the phenotype of ECSHIP2$^{\Delta/+}$ ECs. *A*: SHIP2 shRNA reduced SHIP2 protein by ~75% vs. control shRNA (n = 3; representative Western blot shown above the panel). *B*: SHIP2 activity is reduced by SHIP2 shRNA (n = 3). *C*: Increased superoxide abundance in SHIP2 knockdown HUVECs measured by lucigenin-enhanced chemiluminescence (n = 3). *D*: Increased Nox2 NADPH oxidase protein in SHIP2 knockdown HUVECs (n = 5; representative Western blot shown above the panel). Suppression of excess superoxide production in SHIP2 knockdown HUVECs by the NOX2 inhibitor Gp91ds-tat, which was measured with lucigenin-enhanced chemiluminescence ($n \geq 3$) (*E*) and dihydroethidium (DHE) fluorescence (n = 6) (*F*). *G*: Increased concentration of S473 pAkt and S1177 peNOS in SHIP2 knockdown HUVECs (n = 5). *H*: Suppression of excess superoxide production in SHIP2 knockdown HUVECs by the PI3K inhibitors Wortmannin and LY294002 (n = 5). AU, arbitrary units; ROS, reactive oxygen species; GP-tat, Gp91ds-tat NADPH oxidase 2 inhibitor; WT, Wortmannin; LY, LY294002 PI3K inhibitor. *$P < 0.05$.

SHIP2 modulation on insulin sensitivity in models of type 2 diabetes. Adenoviral expression of a dominant-negative mutant SHIP2 in the liver of obese hyperglycemic mice restored insulin sensitivity and Akt phosphorylation (22), whereas the expression of wild-type SHIP2 blunted these (23). In humans, SHIP2 (*Inppl1*) polymorphisms are associated with obesity, type 2 diabetes, and the metabolic syndrome (24,25). SHIP2 inhibition has thus been suggested as an approach for treating insulin-resistant type 2 diabetes (7). However, the effect of SHIP2 inhibition on specific components of the arterial wall is ill defined; our data question the potential therapeutic benefit of SHIP2 inhibition, at least in the endothelium.

Endothelial SHIP2 Inhibition and Glucose Homeostasis

We demonstrated that 10-month-old ECSHIP2$^{\Delta/+}$ mice were resistant to insulin-mediated glucose lowering, and the vascular dysfunction caused by chronic SHIP2 inactivation may underpin these findings. We found reduced insulin-stimulated eNOS activation in ECSHIP2$^{\Delta/+}$ ECs, and endothelial-derived NO is thought to be crucial for insulin-stimulated glucose uptake; eNOS-deficient mice are systemically insulin resistant, with reduced insulin-mediated glucose uptake in skeletal muscle (26,27). Kubota et al. (28) demonstrated impaired insulin-stimulated glucose disposal in the skeletal muscle of mice with endothelium-specific deletion of IRS2 due to impaired NO bioavailability. Our data sets are consistent with this, since ECSHIP2$^{\Delta/+}$ mice have reduced EC insulin sensitivity, diminished insulin-stimulated glucose uptake to skeletal muscle, and reduced endothelial NO generation. However, mice with endothelium-specific insulin receptor deletion have normal glucose disposal during clamping studies (29), suggesting a complex association between vascular insulin signaling and systemic glucose homeostasis. Importantly, ECSHIP2$^{\Delta/+}$ mice had preserved proximal insulin signaling, implying that downstream signaling may be more important in vascular homeostasis, including the regulation of systemic glucose metabolism.

Endothelial SHIP2 Inhibition, Superoxide Generation, and eNOS Inhibition

We demonstrate that EC-specific inactivation of SHIP2 increases basal activation of the PI3K/Akt/eNOS signaling cascade, with potentially important increases in both the total and phosphorylated forms of key signaling nodes (which did not increase in response to insulin), and increases the abundance

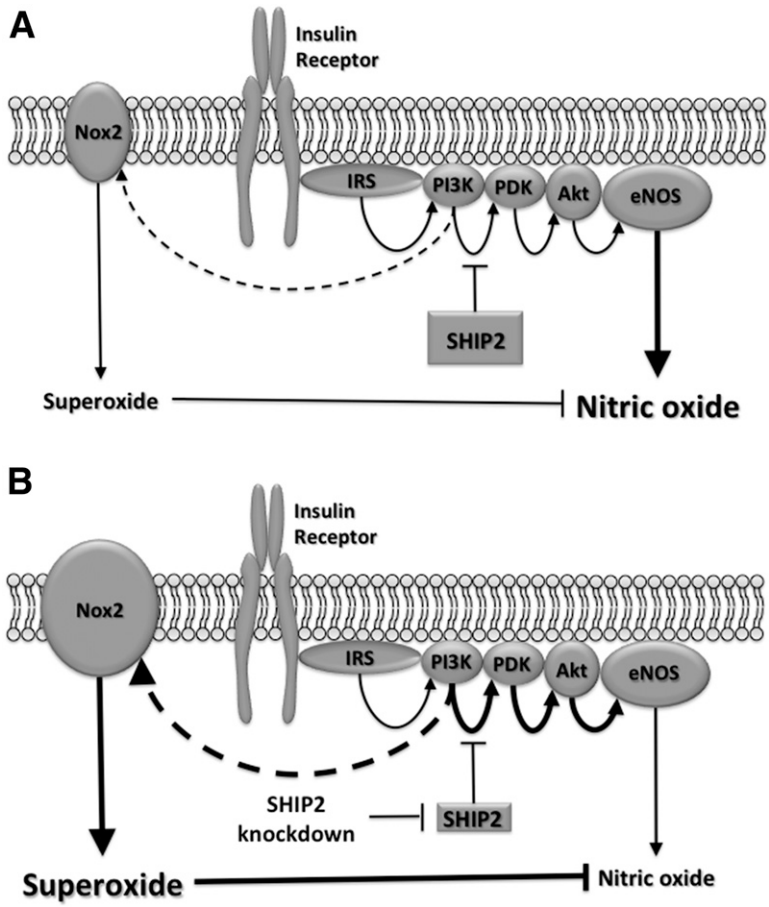

Figure 8—Proposed mechanism of endothelial dysfunction associated with SHIP2 knockdown. In contrast with normal physiology (*A*), reduced SHIP2 activity (*B*) results in increased basal PI3K/Akt/eNOS signaling, although NOX2 is also hyperactivated, resulting in oxidative stress and reduced NO bioavailability.

of superoxide. This is associated with reduced NO production in isolated ECs and aortic segments under isometric tension, indicating endothelial dysfunction. The expression of Nox2 NADPH oxidase was increased in the setting of SHIP2 knockdown, and by using the selective antagonist Gp91ds-tat we implicated Nox2 as the source of excess superoxide. Moreover, by normalizing superoxide abundance using two selective PI3K inhibitors, we also implicated excessive PI3K/Akt signaling as contributing to oxidative stress. Although a number of studies have shown a link between excessive Akt activation and superoxide generation (30,31), none have identified the source of excess superoxide. Moreover, the association between SHIP2 and oxidative stress in vivo is currently unexplored. Our study is therefore the first to mechanistically link SHIP2 inactivation to increased Nox2 NADPH oxidase activity, oxidative stress, and endothelial dysfunction (Fig. 8). By recapitulating these data in human ECs after silencing SHIP2, we provide support for the relevance of our in vivo observations to human pathophysiology, suggesting that caution is warranted in the clinical translation of SHIP2 inhibition. Importantly, we have also published (12) that mice with endothelial overexpression of the insulin receptor exhibit many of the phenotypic traits noted in ECSHIP2$^{\Delta/+}$ mice, including PI3K- and Nox2-dependent vascular oxidative stress and endothelial dysfunction. In conjunction, these data suggest that unrestrained signaling at multiple nodes in the proximal insulin signaling cascade cause vascular dysfunction mediated by Nox2-dependent oxidative stress.

Conclusion

Vascular endothelial SHIP2 activity is required to maintain normal systemic insulin sensitivity and suppress vascular oxidative stress and endothelial dysfunction caused by unrestrained PI3K-Nox2 signaling.

Funding. This work was supported by British Heart Foundation grant RG09/010. P.A.P. and A.M.N.W. are supported by a British Heart Foundation Clinical Research Training Fellowships. D.J.B. is a Wellcome Trust Investigator. S.B.W. is supported by European Research Council starter award 310747. M.T.K. is British Heart Foundation Professor of Cardiovascular and Diabetes Research. R.M.C. is supported by British Heart Foundation Intermediate Research Fellowship FS/12/80/29821.

Duality of Interest. No potential conflicts of interest relevant to this article were reported.

Author Contributions. N.T.W., P.A.P., and R.M.C. collected data and wrote the manuscript. M.C.G., H.V., P.S., S.G., N.Y.Y., H.I., A.M.N.W., K.J.G., N.M., A.S., and K.B. collected data. D.J.B. and S.B.W. contributed to discussion and reviewed and edited the manuscript. S.S. provided materials, contributed to discussion, and reviewed and edited the manuscript. M.T.K. wrote the manuscript. M.T.K. is the guarantor of this work and, as such, had full access to all the data in the study and takes responsibility for the integrity of the data and the accuracy of the data analysis.

References

1. Johnson AMF, Olefsky JM. The origins and drivers of insulin resistance. Cell 2013;152:673–684

2. Duncan ER, Walker SJ, Ezzat VA, et al. Accelerated endothelial dysfunction in mild prediabetic insulin resistance: the early role of reactive oxygen species. Am J Physiol Endocrinol Metab 2007;293:E1311–E1319

3. Wheatcroft SB, Shah AM, Li J-M, et al. Preserved glucoregulation but attenuation of the vascular actions of insulin in mice heterozygous for knockout of the insulin receptor. Diabetes 2004;53:2645–2652

4. Sukumar P, Viswambharan H, Imrie H, et al. Nox2 NADPH oxidase has a critical role in insulin resistance-related endothelial cell dysfunction. Diabetes 2013;62:2130–2134

5. Duncan ER, Crossey PA, Walker S, et al. Effect of endothelium-specific insulin resistance on endothelial function in vivo. Diabetes 2008;57:3307–3314

6. Noronha BT, Li JM, Wheatcroft SB, Shah AM, Kearney MT. Inducible nitric oxide synthase has divergent effects on vascular and metabolic function in obesity. Diabetes 2005;54:1082–1089

7. Lazar DF, Saltiel AR. Lipid phosphatases as drug discovery targets for type 2 diabetes. Nat Rev Drug Discov 2006;5:333–342

8. Kagawa S, Soeda Y, Ishihara H, et al. Impact of transgenic overexpression of SH2-containing inositol 5′-phosphatase 2 on glucose metabolism and insulin signaling in mice. Endocrinology 2008;149:642–650

9. Clément S, Krause U, Desmedt F, et al. The lipid phosphatase SHIP2 controls insulin sensitivity. Nature 2001;409:92–97

10. Sleeman MW, Wortley KE, Lai K-MV, et al. Absence of the lipid phosphatase SHIP2 confers resistance to dietary obesity. Nat Med 2005;11:199–205

11. Dubois E, Jacoby M, Blockmans M, et al. Developmental defects and rescue from glucose intolerance of a catalytically-inactive novel Ship2 mutant mouse. Cell Signal 2012;24:1971–1980

12. Viswambharan H, Yuldasheva NY, Sengupta A, et al. Selective Enhancement of Insulin Sensitivity in the Endothelium In Vivo Reveals a Novel Proatherosclerotic Signaling Loop. Circ Res 2017;120:784–798

13. Anderson EJ, Lustig ME, Boyle KE, et al. Mitochondrial H2O2 emission and cellular redox state link excess fat intake to insulin resistance in both rodents and humans. J Clin Invest 2009;119:573–581

14. Abbas A, Imrie H, Viswambharan H, et al. The insulin-like growth factor-1 receptor is a negative regulator of nitric oxide bioavailability and insulin sensitivity in the endothelium. Diabetes 2011;60:2169–2178

15. Imrie H, Viswambharan H, Sukumar P, et al. Novel role of the IGF-1 receptor in endothelial function and repair: studies in endothelium-targeted IGF-1 receptor transgenic mice. Diabetes 2012;61:2359–2368

16. Li J, Hou B, Tumova S, et al. Piezo1 integration of vascular architecture with physiological force. Nature 2014;515:279–282

17. Cubbon RM, Yuldasheva NY, Viswambharan H, et al. Restoring Akt1 activity in outgrowth endothelial cells from South Asian men rescues vascular reparative potential. Stem Cells 2014;32:2714–2723

18. Dalmas E, Toubal A, Alzaid F, et al. Irf5 deficiency in macrophages promotes beneficial adipose tissue expansion and insulin sensitivity during obesity. Nat Med 2015;21:610–618

19. Engelman JA, Luo J, Cantley LC. The evolution of phosphatidylinositol 3-kinases as regulators of growth and metabolism. Nat Rev Genet 2006;7:606–619

20. Manning BD, Cantley LC. AKT/PKB signaling: navigating downstream. Cell 2007;129:1261–1274

21. Taniguchi CM, Emanuelli B, Kahn CR. Critical nodes in signalling pathways: insights into insulin action. Nat Rev Mol Cell Biol 2006;7:85–96

22. Grempler R, Zibrova D, Schoelch C, van Marle A, Rippmann JF, Redemann N. Normalization of prandial blood glucose and improvement of glucose tolerance by liver-specific inhibition of SH2 domain containing inositol phosphatase 2 (SHIP2) in diabetic KKAy mice: SHIP2 inhibition causes insulin-mimetic effects on glycogen metabolism, gluconeogenesis, and glycolysis. Diabetes 2007;56:2235–2241

23. Fukui K, Wada T, Kagawa S, et al. Impact of the liver-specific expression of SHIP2 (SH2-containing inositol 5′-phosphatase 2) on insulin signaling and glucose metabolism in mice. Diabetes 2005;54:1958–1967

24. Marion E, Kaisaki PJ, Pouillon V, et al. The gene INPPL1, encoding the lipid phosphatase SHIP2, is a candidate for type 2 diabetes in rat and man. Diabetes 2002;51:2012–2017

25. Kaisaki PJ, Delépine M, Woon PY, et al. Polymorphisms in type II SH2 domain-containing inositol 5-phosphatase (INPPL1, SHIP2) are associated with physiological abnormalities of the metabolic syndrome. Diabetes 2004;53:1900–1904
26. Duplain H, Burcelin R, Sartori C, et al. Insulin resistance, hyperlipidemia, and hypertension in mice lacking endothelial nitric oxide synthase. Circulation 2001;104:342–345
27. Shankar RR, Wu Y, Shen HQ, Zhu JS, Baron AD. Mice with gene disruption of both endothelial and neuronal nitric oxide synthase exhibit insulin resistance. Diabetes 2000;49:684–687
28. Kubota T, Kubota N, Kumagai H, et al. Impaired insulin signaling in endothelial cells reduces insulin-induced glucose uptake by skeletal muscle. Cell Metab 2011;13:294–307
29. Vicent D, Ilany J, Kondo T, et al. The role of endothelial insulin signaling in the regulation of vascular tone and insulin resistance. J Clin Invest 2003;111:1373–1380
30. Wang C-Y, Kim H-H, Hiroi Y, et al. Obesity increases vascular senescence and susceptibility to ischemic injury through chronic activation of Akt and mTOR. Sci Signal 2009;2:ra11
31. Kerr BA, Ma L, West XZ, et al. Interference with akt signaling protects against myocardial infarction and death by limiting the consequences of oxidative stress. Sci Signal 2013;6:ra67